American Mineralogist, Volume 99, pages 2171–2175, 2014

MINERALS IN THE HUMAN BODY

Thermal expansion of fluorapatite-hydroxylapatite crystalline solutions† 🔓

Guy L. Hovis[1,*], Brian T. Scott[1], Caitlin M. Altomare[1], Amanda R. Leaman[1], Matthew D. Morris[1], Gary P. Tomaino[2] and Francis M. McCubbin[3]

[1]Department of Geology and Environmental Geosciences, Lafayette College, Easton, Pennsylvania 18042, U.S.A.
[2]Specialty Minerals Inc., 640 North Thirteenth Street, Easton, Pennsylvania 18042, U.S.A.
[3]Institute of Meteoritics, Department of Earth and Planetary Sciences, University of New Mexico, Albuquerque, New Mexico 87131, U.S.A.

Abstract

Fluorapatite has been synthesized through ion-exchange between NIST hydroxylapatite SRM 2910a and optical-grade fluorite. The latter end-member and additional intermediate F-OH apatite samples made through ion-exchange between the newly synthesized fluorapatite and the original hydroxylapatite have provided materials for an investigation of thermal expansion in the F-OH apatite system. Unit-cell volumes determined from X-ray powder diffraction data collected between 22 and 928 °C have been utilized to compute the coefficients of thermal expansion at a pressure of 1 bar for seven apatite samples having various F:OH ratios, as well as for natural samples of fluorapatite and hydroxylapatite. Results show that the thermal expansion coefficient for volume averages 41.0 ± 1.4 (1σ) × 10^{-6} deg^{-1} for all samples and is thus little affected by F:OH ratio. This study extends the thermodynamic characterization of this important mineral system, with potential applications for the geological, planetary, biological, medical, and materials-science communities.

Keywords: Fluorapatite, hydroxylapatite, F-OH apatite, thermal expansion

Introduction

Apatite, $A_5(XO_4)_3Z$, is a common mineral in igneous, metamorphic, and sedimentary rocks. It can be found in planetary materials as well (Piccoli and Candela 2002; Spear and Pyle 2002; Knudsen and Gunter 2002; Patiño Douce and Roden 2006; Jones et al. 2014), and in fact has been used to estimate abundances of H_2O in the interiors of the Moon and Mars (McCubbin et al. 2010a, 2012; Gross et al. 2013). Apatite is also a significant component in many fertilizers, an important material for nuclear waste storage (Hughes and Rakovan 2002; Ewing and Wang 2002), and the primary mineral composing solid parts of the human anatomy (Gross and Berndt 2002). As such, it has the potential to yield valuable information to the geological, biological, medical, planetary, and materials-science communities. Despite the broad range of its application, surprisingly little is known regarding the thermodynamics of apatite-group minerals. Consequently, it is of interest to characterize the thermodynamic behavior of minerals in the greater apatite system, as well as its individual subsystems.

For naturally occurring apatites, the primary occupants of the A and X sites are Ca^{2+} and P^{5+}, respectively. However, the mineral varies widely in composition with continuous substitutions of F^-, Cl^-, and $(OH)^-$ in the Z site, as well as limited substitutions of REE^{3+}, Sr^{2+}, Na^+ (among others) for Ca^{2+} in A, and $(CO_3)^{2-}$, S^{2-}, or simply O^{2-} in Z (Pan and Fleet 2002; Hovis and Harlov 2010; Boyce et al. 2010). There also are many minor substitutions such as S^{6+}, Si^{4+}, and C^{4+} for P^{5+} in X. Initial work on thermodynamic characterization focused on F-Cl apatites (Hovis and Harlov 2010). More recently, Hovis et al. (2014) supplemented the latter with a study of the enthalpy and volume characteristics of a newly synthesized F-OH apatite series. Investigation of this series continues in the present work.

Methodology

Sample synthesis and characterization

Synthesis of the present samples has been described in the previous paper on these minerals (Hovis et al. 2014) and builds upon ion-exchange techniques utilized in previous work on other mineral systems such as feldspars (e.g., Hovis 1988; Hovis and Roux 2008) and feldspathoids (e.g., Hovis and Roux 1993; Hovis et al. 2003, 2006). To summarize briefly, NIST special reference material 2910a hydroxylapatite was utilized as the base material to make a series of F-OH apatite solid solutions. The NIST hydroxylapatite was synthesized via solution reaction of calcium hydroxide and phosphoric acid at atmospheric pressure and a temperature near 100 °C; details in the certificate of analysis refer to the synthesis procedure of McDowell et al. (1977). Fluorapatite was made at Lafayette College by tamping down a thin layer of 2910a hydroxylapatite powder on a 50 mm diameter disk of optical-grade fluorite, then holding the disk in air at 750 °C for three days. The resulting F-rich apatite powder then was applied to a fresh fluorite surface and held at the same temperature for an additional three days. This double exchange resulted in a fluorapatite specimen containing ~85 mol% fluorapatite component. Successful ion exchange in the experiments was gauged through examination of the run products using X-ray powder diffraction, which showed well-defined changes in peak position from hydroxylapatite to fluorapatite; the resulting X-ray data also matched that of fluorapatite in the database of the International Center for Diffraction Data (ICDD). Subsequently, intermediate F-OH apatite compositions were synthesized by combining in various proportions 2910a hydroxylapatite and the newly synthesized fluorapatite powders, annealing these for three days at 750 °C, with daily mixing of each powder. Detailed synthesis conditions for all samples are summarized in Table 1 of Hovis et al. (2014).

Chemical characterization of all synthetic F-OH apatite specimens was done by

* E-mail: hovisguy@lafayette.edu

† 🔓 Open access: Article available to all readers online. Special collection papers can be found on GSW at http://ammin.geoscienceworld.org/site/misc/specialissuelist.xhtml.

0003-004X/14/1112–2171$05.00/DOI: http://dx.doi.org/10.2138/am-2014-4914

Table 1. Chemical analysis of hydroxylapatite from Holly Springs, Georgia, U.S.A. (NMNH R9498)

Oxide (wt%)	(N = 25)	Structural formulas based on 13 anions	
P_2O_5	42.49(20)	P	3.00
SiO_2	b.d.	Si	0.00
TiO_2	b.d.	Ti	0.00
Al_2O_3	b.d.	Al	0.00
FeO	0.04(2)	Fe	0.00
MnO	0.05(1)	Mn	0.00
MgO	0.03(3)	Mg	0.00
CaO	55.98(17)	Ca	5.00
Na_2O	0.02(1)	Na	0.00
SO_3	0.01(1)	S	0.00
H_2O[a]	1.61(3)	∑ Cations	8.00
F	0.36(2)	F	0.09
Cl	0.27(3)	Cl	0.04
–O≡F	0.15	OH[a]	0.89
–O≡Cl	0.06	∑ Anions	1.02
Total	100.59	OH[b]	0.87

Notes: 1σ standard deviations for each of the values are provided parenthetically. N = number of analyses per average.
[a] Measured by continuous flow mass spectrometry (N = 3).
[b] Calculated assuming that 1 – Cl – F = OH apfu.

Francis McCubbin at the University of New Mexico using continuous flow mass spectrometry for H_2O determination and electron probe microanalysis for fluorine. The latter utilized special techniques applicable to fine powders, as described in detail and reported in Table 2 of the previous paper (ibid; related references include Stormer et al. 1993; Goldoff et al. 2012; McCubbin et al. 2010b, 2011).

In addition to the synthetic F-OH apatite samples, two natural apatite specimens were obtained from the National Museum of Natural History (Smithsonian Institution) for this investigation, fluorapatite NMNH 144954-3 from Durango (Mexico) with composition $(Ca_{4.90}Na_{0.04}Ce_{0.02})(P_{2.98}Si_{0.02}S_{0.02}O_{12})(F_{0.92}Cl_{0.06}OH_{0.03})$ (Table 2 of Hovis et al. 2014; Young et al. 1969) and hydroxylapatite NMNH R9498 from Holly Springs, Georgia, of composition $(Ca_{5.00})(P_{3.00}O_{12})(F_{0.09}Cl_{0.04}OH_{0.89})$ (Table 1, this study; Hughes et al. 1989). As natural samples, each of the latter strays somewhat from the F-OH apatite binary system.

Initial room-temperature X-ray examination of the samples was done on a Scintag PAD V X-ray powder diffractometer. Scans using Cu radiation typically were run from 15 to 72° 2Θ at a rate of 0.25°/min. NIST 640a silicon, with a stated unit-cell dimension of 5.430825 Å, was used as an internal standard. Analysis of the hydroxylapatite X-ray diffraction pattern was aided by comparison with XRD data given in the NIST certificate of analysis. There also are multiple additional sources of XRD data for fluorapatite and hydroxylapatite, such as the ICDD database. Additionally, it was possible to track peaks from the OH to the F end of the ion-exchange series, and vica versa; this was helpful especially for peak indexing at mid-compositions where XRD data are sparse. Calculations of unit-cell dimensions utilized the unit-cell software of Holland and Redfern (1997).

High-temperature X-ray powder diffraction measurements

High-temperature X-ray powder diffraction measurements on the synthetic F-OH apatite samples were made at Specialty Minerals, Inc., Easton, Pennsylvania, utilizing a Rigaku Ultima Theta-Theta diffractometer in conjunction with a high-temperature stage. Sample temperatures were evaluated in a separate set of experiments using reversible phase transformations for KNO_3, $KClO_4$, K_2SO_4, K_2CrO_4, $BaCO_3$, and $SrCO_3$; collectively, this resulted in temperature calibration from 130 to 930 °C. Based on these experiments, it is estimated that the set-point temperatures for the XRD measurements are known to ±15 °C.

High-temperature X-ray measurements on the two natural apatite specimens were made at Lafayette College utilizing a newly received PANalytical Empyrean Theta-Theta XRD system, with PIXEL3D detector and an Anton-Parr HTK 1200N high-temperature stage that enabled sample height adjustment. Temperatures for this stage too were calibrated using the methodology described above for samples of KNO_3, $KClO_4$, K_2SO_4, and $BaCO_3$; actual temperatures are thought to be within 20 °C of the stated values.

Unit-cell dimension calculations (again utilizing the software of Holland and Redfern 1997) based on both Rigaku and PANalytical data utilized NIST SRM 640a silicon as an internal standard, as well as the high-temperature Si data of Parrish (1953). X-ray peak positions at room temperature were easily tracked for scans at elevated temperatures.

Results

Unit-cell dimensions and volumes

Generally, apatite is a hexagonal mineral with $P6_3/m$ space group symmetry. Various hydroxylapatite samples, however, have been found to display either the latter or monoclinic $P2_1/b$ symmetry (Mackie et al. 1972; Elliott et al. 1973). In single-crystal work, Hughes et al. (1989) found NMNH R9498 hydroxylapatite, used in the present study, to display true hexagonal symmetry. There is no guarantee, however, that synthetic NIST 2910a hydroxylapatite has equivalent symmetry, even though the X-ray powder diffraction pattern indicates this to be the case. Because the β interaxial angle in monoclinic hydroxylapatite is extremely close to 120° (beyond resolution of the determined unit-cell parameters), distinction between the two symmetries can be impossible using X-ray powder diffraction techniques. For purposes here, it has been assumed that NIST 2910a sample is hexagonal, understanding that this is an uncertainty that cannot be resolved with techniques used in the present work.

Unit-cell dimensions *a* and *c*, as well as unit-cell volume, are presented for all specimens and temperatures in Tables 2a and 2b and plotted in Figures 1 to 3. Compositions (mole fractions F) for all synthetic samples are included in Table 3; the bulk composition of hydroxylapatite NMNH R9498 was given earlier in Table 1.

In Figure 1, one sees impressive parallelism of the *a* dimension with temperature among all synthetic F-OH apatite specimens. Data for both of the natural apatite samples fit well with those for the synthetic materials. Note that near-end-member Durango fluorapatite data occur among mid-compositional members of the F-OH synthetic series; offset of data from other F-rich apatites can be attributed to non-binary chemical components. Although some series exhibit slightly curved relationships between *a* and *T*, comparison of linear fits to all data produces closely grouped thermal expansion coefficients for *a* (α_a) (calculated similarly to those for volume given by Eq. 1 below) that average 13.6 ± 0.5 (1σ) × 10^{-6} deg^{-1}, reflecting a very small spread in the data. The parallelism of data in Figure 2 is the first hint that the Z-site anion makes little difference in the expansion behavior of these minerals.

The *c* unit-cell dimension is little affected by F:OH ratio (Hovis et al. 2014), as values across the F-OH series at room temperature are within 0.01 Å of one another, which explains the bunching of data in Figure 2. Data for NMNH R9498 Holly Springs hydroxylapatite falls slightly below other data, again the result of non-binary constituents. The latter do not seem to have affected $\Delta c/\Delta T$ slopes, however, and thermal coefficients for the *c* axis based on linear fits to *c*-*T* data average 13.2 ± 0.7 (1σ) × 10^{-6} deg^{-1}, again showing only a small range in the data. Overall, then, the fractional changes of *a* and *c* with temperature are the same, as reflected by the respective thermal expansion coefficients.

Unit-cell volume data are plotted in Figure 3. Statistics presented in Table 3 illustrate that in some cases linear and quadratic fits to *V*-*T* relations are statistically equivalent, whereas in others quadratic fits are slightly better. For all nine series, linear least-squares fits to the data give R^2 values ≥0.996. For series where quadratic fits are statistically justified, concave-up relationships

TABLE 2a. Unit-cell dimensions and volumes with temperature for synthetic F-OH apatite specimens

	1121			1132			1128			1125		
T (°C)	*a* (Å)	*c* (Å)	*V* (Å³)	*a* (Å)	*c* (Å)	*V* (Å³)	*a* (Å)	*c* (Å)	*V* (Å³)	*a* (Å)	*c* (Å)	*V* (Å³)
22	9.4181(7)	6.8823(10)	528.69(9)	9.4105(3)	6.8827(4)	527.86(3)	9.4025(5)	6.8840(7)	527.05(6)	9.3923(9)	6.8840(11)	525.91(11)
100	9.4250(8)	6.8865(12)	529.77(11)	9.4195(3)	6.8882(4)	529.28(3)	9.4138(7)	6.8887(10)	528.69(9)	9.4024(10)	6.8916(12)	527.63(12)
175	9.4361(13)	6.8908(17)	531.36(15)	9.4330(3)	6.8961(4)	531.41(4)	9.4233(9)	6.8958(12)	530.29(12)	9.4138(7)	6.8983(10)	529.42(9)
250	9.4422(12)	6.9004(15)	532.78(14)	9.4399(3)	6.8996(4)	532.47(4)	9.4304(7)	6.9025(9)	531.62(8)	9.4221(7)	6.9048(9)	530.85(9)
325	9.4548 (10)	6.9065(14)	534.68(13)	9.4472(4)	6.9056(4)	533.75(4)	9.4398(10)	6.9057(12)	532.92(12)	9.4325(11)	6.9106(15)	532.47(13)
400	9.4644 (10)	6.9120(13)	536.19(14)	9.4600(4)	6.9163(4)	536.02(4)	9.4507(7)	6.9180(9)	535.11(9)	9.4420(11)	6.9150(14)	533.88(13)
475	9.4737 (12)	6.9207(14)	537.92(14)	9.4646(3)	6.9225(4)	537.02(4)	9.4603(7)	6.9215(7)	536.46(7)	9.4505(10)	6.9215(14)	535.36(12)
550	9.4853 (13)	6.9275(14)	539.77(16)	9.4788(4)	6.9303(4)	539.24(4)	9.4719(11)	6.9274(13)	538.24(13)	9.4598(7)	6.9310(9)	537.14(9)
625	9.4945(11)	6.9333(14)	541.27(13)	9.4895(4)	6.9362(4)	540.93(4)	9.4804(9)	6.9353(12)	539.82(12)	9.4677(11)	6.9348(16)	538.34(14)
700	9.5043(8)	6.9379(9)	542.75(10)	9.4982(4)	6.9450(4)	542.60(4)	9.4865(7)	6.9433(10)	541.15(9)	9.4766(11)	6.9426(15)	539.96(14)
775	9.5175(11)	6.9487(13)	545.11(13)	9.5091(4)	6.9519(4)	544.39(4)	9.4976(8)	6.9487(10)	542.82(10)	9.4856(11)	6.9506(14)	541.60(14)
850	9.5293(15)	6.9573(16)	547.14(18)	9.5173(4)	6.9646(5)	546.32(5)	9.5091(8)	6.9595(11)	544.98(10)	9.4944(13)	6.9591(18)	543.27(17)
925				9.5233(4)	6.9669(4)	547.20(5)	9.5141(12)	6.9651(15)	546.00(16)	9.5064(11)	6.9644(15)	545.06(14)

	1129			1131			1117		
T (°C)	*a* (Å)	*c* (Å)	*V* (Å³)	*a* (Å)	*c* (Å)	*V* (Å³)	*a* (Å)	*c* (Å)	*V* (Å³)
22	9.3842(6)	6.8856(8)	525.13(8)	9.3789(7)	6.8868(10)	524.63(9)	9.3764(12)	6.8921(16)	524.75(15)
100	9.3934(7)	6.8905(10)	526.54(9)	9.3878(10)	6.8924(13)	526.05(12)	9.3855(8)	6.8973(10)	526.17(10)
175	9.4043(7)	6.8972(9)	528.27(8)	9.3965(7)	6.8978(10)	527.44(9)	9.3883(8)	6.8972(10)	526.47(10)
250	9.4114(9)	6.9013(11)	529.38(11)	9.4092(8)	6.9062(11)	529.51(10)	9.3998(9)	6.9025(11)	528.17(11)
325	9.4237(6)	6.9106(8)	531.48(8)	9.4146(7)	6.9107(9)	530.46(9)	9.4058(8)	6.9105(11)	529.45(10)
400	9.4302(10)	6.9169(12)	532.70(12)	9.4259(8)	6.9171(11)	532.22(11)	9.4158(6)	6.9170(8)	531.08(7)
475	9.4402(8)	6.9221(11)	534.22(10)	9.4363(10)	6.9246(13)	533.98(13)	9.4248(9)	6.9215(11)	532.45(22)
550	9.4506(8)	6.9322(10)	536.19(10)	9.4470(13)	6.9325(15)	535.81(15)	9.4347(9)	6.9287(12)	534.12(11)
625	9.4618(9)	6.9374(12)	537.87(11)	9.4537(12)	6.9373(13)	536.93(14)	9.4468(10)	6.9363(12)	536.08(12)
700	9.4728(8)	6.9444(9)	539.67(9)	9.4599(12)	6.9444(15)	538.19(14)	9.4552(10)	6.9447(12)	537.67(12)
775	9.4801(12)	6.9489(12)	540.85(13)	9.4693(13)	6.9508(14)	539.77(15)	9.4630(10)	6.9508(13)	539.04(13)
850	9.4871(10)	6.9583(11)	542.38(12)	9.4806(12)	6.9575(15)	541.57(15)	9.4790(13)	6.9561(14)	541.28(14)
925	9.4950(11)	6.9644(13)	543.75(14)	9.4922(16)	6.9682(15)	543.74(18)	9.4902(11)	6.9631(12)	543.10(13)

Note: Standard errors (1σ) in the last decimal place(s) are given in parentheses.

TABLE 2b. Unit-cell dimensions and volumes with temperature for natural apatite specimens

	NMNH R9498 (Holly Springs hydroxylapatite)			NMNH 144954-3 (Durango fluorapatite)		
T (°C)	*a* (Å)	*c* (Å)	*V* (Å³)	*a* (Å)	*c* (Å)	*V* (Å³)
22	9.4275(3)	6.8768(4)	529.30(3)	9.3930(3)	6.8829(3)	525.91(3)
66	9.4325(3)	6.8797(5)	530.09(4)	9.3980(3)	6.8860(3)	526.71(3)
113	9.4382(2)	6.8832(3)	531.01(3)	9.4035(3)	6.8897(4)	527.60(4)
172	9.4442(3)	6.8871(4)	531.99(4)	9.4101(4)	6.8938(4)	528.66(4)
228	9.4520(4)	6.8917(4)	533.22(4)	9.4162(4)	6.8986(5)	529.72(5)
278	9.4584(3)	6.8962(4)	534.29(4)	9.4231(4)	6.9029(5)	530.82(5)
328	9.4646(4)	6.9000(5)	535.28(4)	9.4291(4)	6.9069(5)	531.81(5)
378	9.4721(4)	6.9049(4)	536.51(4)	9.4354(4)	6.9115(5)	532.87(4)
428	9.4790(3)	6.9096(4)	537.67(4)	9.4421(3)	6.9158(4)	533.97(4)
478	9.4860(4)	6.9146(5)	538.84(4)	9.4490(3)	6.9208(4)	535.14(4)
528	9.4928(2)	6.9191(3)	539.97(2)	9.4550(3)	6.9258(3)	536.20(3)
578	9.4993(3)	6.9240(3)	541.09(3)	9.4620(3)	6.9304(4)	537.34(4)
628	9.5070(3)	6.9293(4)	542.39(4)	9.4690(2)	6.9350(2)	538.50(2)
678	9.5139(3)	6.9346(3)	543.58(3)	9.4760(2)	6.9404(2)	539.71(2)
728	9.5210(3)	6.9405(4)	544.86(4)	9.4827(3)	6.9457(2)	540.89(3)
878	9.5412(4)	6.9587(4)	548.61(4)	9.5042(2)	6.9629(3)	544.70(3)
928	9.5473(4)	6.9652(5)	549.83(5)	9.5124(3)	6.9689(4)	546.10(3)

Note: Standard errors (1σ) in the last decimal place(s) are given in parentheses.

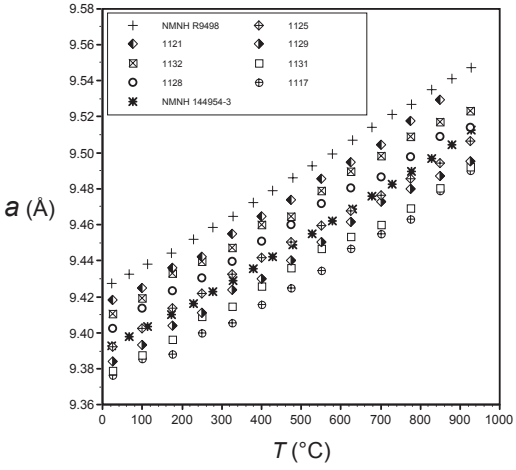

FIGURE 1. Variation of the *a* unit-cell dimension with temperature (°C) for F-OH apatites of the present investigation. Sizes of the symbols equate to about 0.4 Å, many times larger than the standard errors given in Tables 2a and 2b.

are prevalent. Equations for both linear and quadratic relationships are included in Table 3.

To obtain a general picture of the effect of temperature on volume for F-OH apatite, one can focus on linear fits to the *V*-*T* data (Table 3). Thermal expansion coefficients for volume (α_V) have been calculated as

$$\alpha_V(\text{deg}^{-1}) = (\Delta V/\Delta T)V_{0°C} \quad (1)$$

where $\Delta V/\Delta T$ (Å³/°C) are the slopes of the least-squares-fitted *V*-*T* lines and $V_{0°C}$ (Å³) values are the intercepts of those lines at 0 °C. Thermal expansion coefficients for volume average 41.0 ± 1.4 (1σ) × 10^{-6} deg^{-1} (Table 3, Fig. 4) among all series. This reflects the general parallelism of data in Figure 3.

DISCUSSION AND IMPLICATIONS

Thermal expansion coefficients for end-member F- and OH-apatite have been measured previously by Trombe (1973) and also Brunet et al. (1999). Trombe (1973) presents data in graphical (not tabular) form, so comparison with present data is difficult. Brunet et al. (1999) calculated values of α_V from Trombe's data and determined quantities of 40 and 42 ×10^{-6} deg^{-1} for fluroapatite and hydroxylapatite end-members, respectively; these agree well with present data. Brunet et al. (1999) give quadratic, not linear, relationships for their volume data (again in graphical, not tabular, form), which appear to be similar to ours. We have not attempted

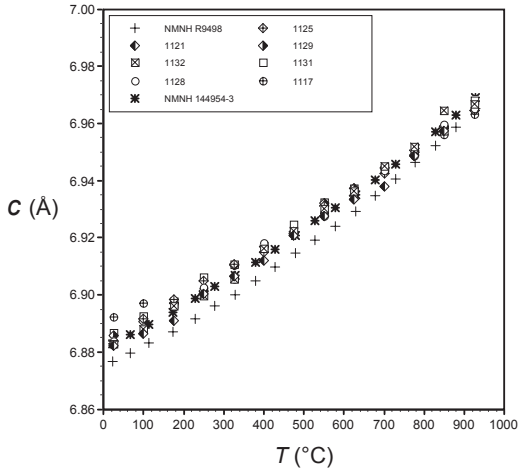

Figure 2. Variation of the *c* unit-cell dimension with temperature (°C) for F-OH apatites of the present investigation. Sizes of the symbols equate to about 0.25 Å, many times larger than the standard errors given in Tables 2a and 2b.

Table 3. Volume-temperature equations for various apatite samples

Sample	Mole fraction F	a_0	a_1	a_2	$\alpha_V \times 10^6$ (deg^{-1})	R^2
1121 linear	0	527.49	0.022382		42.4	0.9968
1121 quadratic	0	528.07	0.018321	4.6407E-06		0.9991
1132 linear	0.118	527.10	0.022064		41.9	0.9976
1132 quadratic	0.118	527.30	0.020730	1.4039E-06		0.9978
1128 linear	0.279	526.43	0.021307		40.5	0.9988
1128 quadratic	0.279	526.54	0.020585	7.5984E-07		0.9989
1125 linear	0.442	525.57	0.020812		39.6	0.9994
1125 quadratic	0.442	525.60	0.020574	2.5071E-07		0.9994
1129 linear	0.594	524.46	0.021123		40.3	0.9987
1129 quadratic	0.594	524.44	0.021261	−1.4543E-07		0.9987
1131 linear	0.720	523.95	0.020862		39.8	0.9980
1131 quadratic	0.720	524.05	0.020242	6.5312E-07		0.9980
1117 linear	0.85	523.29	0.020568		39.3	0.9913
1117 quadratic	0.85	524.33	0.013872	7.0486E-06		0.9985
NMNH R9498 linear	0.09	528.15	0.022891		43.3	0.9978
NMNH R9498 quadratic	0.09	528.77	0.018891	4.2266E-06		0.9998
NMNH 144954-3 linear	0.92	524.81	0.022198		42.3	0.9972
NMNH 144954-3 quadratic	0.92	525.51	0.017692	4.7625E-06		0.9999

Note: Equations have the form: V (Å^3/unit cell) = $a_0 + a_1 T + a_2 T^2$, where temperature (T) is expressed in °C.

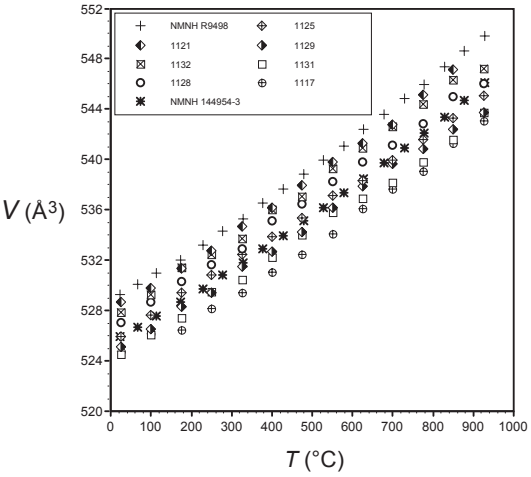

Figure 3. Unit-cell volume as a function of temperature (°C) for F-OH apatites of the present investigation. Note that natural samples have substitutions beyond the binary system. Sizes of the symbols equate to about 1 Å^3, many times larger than the standard errors given in Tables 2a and 2b. Many series display non-linear relationships that nevertheless are close to linear. Both linear and quadratic equations for *V*-*T* relationships are given in Table 3.

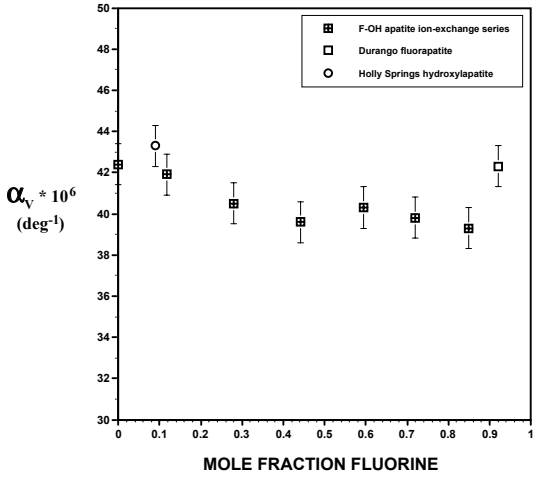

Figure 4. Thermal expansion coefficients for volume calculated according to Equation 1. Error bars of ±1 α_V unit (deg^{-1}) provide a means of comparison for all data and are based simply on the overall variation in α_V among all samples.

to reinterpret their data as linear relationships.

The object of this study was to determine whether the Z-site anions, in this case F^- vs. $(OH)^-$, make a difference in the degree to which apatite expands when it is heated. The plot in Figure 3 and the resulting thermal expansion coefficients (Table 3, Fig. 4) indicate that it does not. In thinking about possible explanations for this, one must consider the nature of the anion (F, OH, Cl) position(s) in the apatite structure. In fact, the latter constitutes one of six ions that coordinate the so-designated Ca(2) position in the apatite structure (Hughes et al. 1989; also see Hughes and Rakovan 2002, for multiple additional references), the remaining five ions being O^{2-}. The lower charge of $(F/OH/Cl)^-$ ions compared with O^{2-} should result in a relatively weaker bond with Ca^{2+}. One might expect a $(F/OH/Cl)^-$ ion, therefore, to have a relatively large degree of vibrational freedom, regardless of which anion occupies this position. When one considers that F^- and $(OH)^-$ have essentially the same radius [reflected by room-temperature apatite volumes, where the substitution of $(OH)^-$ by F^- reduces unit-cell volume by only ~1%; Hovis et al. 2014], the similar thermal behavior of the two entities seems all the more reasonable. Even if two anions were different in size, however, the relatively weak Ca^{2+}-anion bond could perhaps accommodate the size difference through vibrational flexibility.

Study of the thermal expansion behavior of F-OH apatite adds to the thermodynamic database for apatite solid solutions. For room temperature, Hovis et al. (2014) concluded from the linear relationship of unit-cell volume with composition for these same

samples (their Fig. 3) that volumes of F-OH mixing (V_{ex}) are nonexistent. That thermal expansion coefficients are essentially the same across the fluorapatite-hydroxylapatite series now extends the $V_{ex} = 0$ relationship to temperatures above 900 °C and also makes the calculation of high-temperature volumes for any F-OH apatite solid solution quite easy.

Present data on F-OH apatite along with recent data on F-Cl apatite (Hovis and Harlov 2010) add significantly to the thermodynamic database for the apatite system, but there still is much work to do. The apatite Cl-OH binary and F-Cl-OH ternary systems remain thermodynamically uncharacterized. Thermodynamic quantification of substitutions such as $(CO_3)^{2-}$ and O^{2-} in the anion sites, Na^+ and Sr^{2+} for Ca^{2+} in the cation sites, and structural H_2O molecules (Mason et al. 2009; Yoder et al. 2012) remain on the "to do" list for this system. Given the widespread occurrence of apatite in igneous and metamorphic rocks and its potential to contribute substantially to the interpretation of rock petrogenesis, further thermodynamic characterization of this complex system seems likely to produce highly valuable data. When samples become available, our laboratory will be pleased to contribute further to this endeavor.

Acknowledgments

G.L.H. thanks the Earth Sciences Division of the U.S. National Science Foundation for support of this research through Earth Science Instruments and Facilities grant EAR-1028953, which was responsible for purchase of our PANalytical Empyrean XRD unit, with heating stage, and also research grant EAR-1019809, which included support for student research on these minerals. G.L.H. is grateful not only for support of present projects, but also for the support of undergraduate research over many years; indeed, several undergraduates are coauthors of this work. F.M.M. acknowledges support from NASA's Cosmochemistry program through grant NNX11AG76G.

References cited

Boyce, J.W., Liu, Y., Rossman, G.R., Guan, Y., Eiler, J.M., Stolper, E.M., and Taylor, L.A. (2010) Lunar apatite with terrestrial volatile abundances. Nature, 466, 466–469.

Brunet, F., Allan, D.R., Redfern, S.A.T., Angel, R.J., Miletich, R., Reichman, H.J., Sergent, J., and Hanfland, M. (1999) Compressibility and thermal expansivity of synthetic apatites $Ca_5(PO_4)_3X$ with X = OH, F, and Cl. European Journal of Mineralogy, 11, 1023–1035.

Elliott, J.C., Mackie, P.E., and Young, R.A. (1973) Monoclinic hydroxylapatite. Science, 80, 1055–1057.

Ewing, R.C., and Wang, L.M. (2002) Phosphates as nuclear waste forms. In M.J. Kohn, J. Rakovan, and J.M. Hughes, Eds., Phosphates: Geochemical, Geobiological, and Materials Importance, 48, p. 673–699. Reviews in Mineralogy and Geochemistry, Mineralogical Society of America, Chantilly, Virginia.

Goldoff, B., Webster, J.D., and Harlov, D.E. (2012) Characterization of fluor-chlorapatites by electron probe microanalysis with a focus on time-dependent intensity variation of halogens. American Mineralogist, 97, 1103–1115.

Gross, K.A., and Berndt, C.C. (2002) Compositions of the apatitegroup minerals: Substitution mechanisms and controlling factors. In M.J. Kohn, J. Rakovan, and J.M. Hughes, Eds., Phosphates: Geochemical, Geobiological, and Materials Importance, 48, p. 631–672. Reviews in Mineralogy and Geochemistry, Mineralogical Society of America, Chantilly, Virginia.

Gross, J., Filiberto, J., and Bell, A.S. (2013) Water in the martian interior: Evidence for terrestrial MORB mantle-like volatile contents from hydroxyl-rich apatite in olivine-phyric shergottite NWA 6234. Earth and Planetary Science Letters, 369, 120–128.

Holland, T.J.B., and Redfern, S.A.T. (1997) Unit-cell refinement: Changing the dependent variable, and use of regression diagnostics. Mineralogical Magazine, 61, 65–77.

Hovis, G.L. (1988) Enthalpies and volumes related to K-Na mixing and Al-Si order/disorder in alkali feldspars. Journal of Petrology, 29, 731–763.

Hovis, G.L., and Harlov, D. (2010) Solution calorimetric investigation of fluor-chlorapatite crystalline solutions. American Mineralogist, 95, 946–952.

Hovis, G.L., and Roux, J. (1993) Thermodynamic mixing properties of nepheline—kalsilite crystalline solutions. American Journal of Science, 293, 1108–1127.

——— (2008) Thermodynamic mixing properties of Rb-K feldspars. American Mineralogist, 93, 1597–1602.

Hovis, G.L., Crelling, J., Wattles, D., Dreibelbis, B., Dennison, A., Keohane, M., and Brennan, S. (2003) Thermal expansion of nepheline–kalsilite crystalline solutions. Mineralogical Magazine, 67, 535–546.

Hovis, G.L., Person, E., Spooner, A., and Roux, J. (2006) Thermal expansion of highly silicic nepheline-kalsilite crystalline solutions. Mineralogical Magazine, 70, 383–396.

Hovis, G.L., McCubbin, F.M., Nekvasil, H., Ustunisik, G., Woerner, W.R., and Lindsley, D.H. (2014) A novel technique for fluorapatite synthesis and the thermodynamic mixing behavior of F-OH apatite crystalline solutions. American Mineralogist, 99, 890–897.

Hughes, J.M., and Rakovan, J. (2002) The crystal structure of apatite. In M.J. Kohn, J. Rakovan, and J.M. Hughes, Eds., Phosphates: Geochemical, Geobiological, and Materials Importance, 48, p. 1–12. Reviews in Mineralogy and Geochemistry, Mineralogical Society of America, Chantilly, Virginia.

Hughes, J.M., Cameron, M., and Crowley, K.D. (1989) Structural variations in natural F, OH, and Cl apatites. American Mineralogist, 74, 870–876.

Jones, R.H., McCubbin, F.M., Dreeland, L., Guan, Y., Burger, P.V., and Shearer, C.K. (2014) Phosphate minerals in LL chondrites: A record of the action of fluids during metamorphism on ordinary chondrite parent bodies. Geochimica et Cosmochimica Acta, 132, 120–140.

Knudsen, A.C., and Gunter, M.E. (2002) Sedimentary phosphorites—An example: Phosphoria formation, southeastern Idaho, USA. In M.J. Kohn, J. Rakovan, and J.M. Hughes, Eds., Phosphates: Geochemical, Geobiological, and Materials Importance, 48, p. 363−390. Reviews in Mineralogy and Geochemistry, Mineralogical Society of America, Chantilly, Virginia.

Mackie, P.E., Elliott, J.C., and Young, R.A. (1972) Monoclinic structure of synthetic $Ca_5(PO)_4Cl$, chlorapatite. Acta Crystallographia B, 28, 1840–1848.

Mason, H.E., McCubbin, F.M., Smirnov, A., and Phillips, B.L. (2009) Solid-state NMR and IR spectroscopic investigation of the role of structural water and F in carbonate-rich fluorapatite. American Mineralogist, 94, 507–516.

McCubbin, F.M., Steele, A., Hauri, E.H., Nekvasil, H., Yamashita, S., and Hemley, R.J. (2010a) Nominally hydrous magmatism on the Moon. Proceedings of the National Academy of Sciences, 107, 11223–11228.

McCubbin, F.M., Steele, A., Nekvasil, H., Schnieders, A., Rose, T., Fries, M., Carpenter, P.K., and Jolliff, B.L. (2010b) Detection of structurally bound hydroxyl in fluorapatite from Apollo mare basalt 15058,128 using TOF-SIMS. American Mineralogist, 95, 1141–1150.

McCubbin, F.M., Jolliff, B.L., Nekvasil, H., Carpenter, P.K., Zeigler, R.A., Steele, A., Elardo, S.M., and Lindsley, D.H. (2011) Fluorine and chlorine abundances in lunar apatite: Implications for heterogeneous distributions of magmatic volatiles in the lunar interior. Geochimica et Cosmochimica Acta, 75, 5073–5093.

McCubbin, F.M., Hauri, E.H., Elardo, S.M., Vander Kaaden, K.E., Wang, J., Shearer, C.K. (2012) Hydrous melting of the martian mantle produced both depleted and enriched shergottites. Geology, 40, 683–686.

McDowell, H., Gregory, T.M., and Brown, W.E. (1977) Solubility of $Ca_5(PO_4)_3OH$ in the system $Ca(OH)_2$-H_3PO_4-H_2O at 5, 15, 25 and 37 °C. Journal of Research of the National Bureau of Standards, 81A, 273–281.

Pan, Y., and Fleet, M.E. (2002) Compositions of the apatite-group minerals: Substitution mechanisms and controlling factors. In M.J. Kohn, J. Rakovan, and J.M. Hughes, Eds., Phosphates: Geochemical, Geobiological, and Materials Importance, 48, p. 13–50. Reviews in Mineralogy and Geochemistry, Mineralogical Society of America, Chantilly, Virginia.

Parrish, W. (1953) X-ray reflection angle tables for several standards. Technical Report No. 68, Philips Laboratories Incorporated, Irvington on Hudson, New York.

Patiño Douce, A.E., and Roden, M.F. (2006) Apatite as a probe of halogen and water fugacities in the terrestrial planets. Geochimica et Cosmochimica Acta, 70, 3173–3196.

Piccoli, P.M., and Candela, P.A. (2002) Apatite in igneous systems. In M.J. Kohn, J. Rakovan, and J.M. Hughes, Eds., Phosphates: Geochemical, Geobiological, and Materials Importance, 48, p. 255–292. Reviews in Mineralogy and Geochemistry, Mineralogical Society of America, Chantilly, Virginia.

Spear, F.S., and Pyle, J.M. (2002) Apatite, monazite, and xenotime in metamorphic rocks. In M.J. Kohn, J. Rakovan, and J.M. Hughes, Eds., Phosphates: Geochemical, Geobiological, and Materials Importance, 48, p. 293–336. Reviews in Mineralogy and Geochemistry, Mineralogical Society of America, Chantilly, Virginia.

Stormer, J.C., Pierson, M.L., and Tacker, R.C. (1993) Variation of F-X-ray and Cl-X-ray intensity due to anisotropic diffusion in apatite during electron-microprobe analysis. American Mineralogist, 78, 641–648.

Trombe, J.-C. (1973) Contribution à l'étude de la décomposition et de la réactivité de certaines apatites hydroxylées et carbonatées. Annales de Chimie, 8, 251–269.

Yoder, C.H., Pasteris, J.D., Worcester, K.N., and Schermerhorn, D.V. (2012) Structural water in carbonated hydroxylapatite and fluorapatite: Confirmation by solid state ^2H NMR. Calcified Tissue International, 90, 60–67.

Young, E.J, Myers, A.T., Munson, E.L., and Conklin, N.M. (1969) Mineralogy and geochemistry of fluorapatite from Cerro de Mercado, Durango, Mexico. U.S. Geological Survey Professional Paper 650-D, D84–D93.

Manuscript received February 2, 2014
Manuscript accepted June 23, 2014
Manuscript handled by Gregory Meeker